J Comput Aided Mol Des (2013) 27:681–688
DOI 10.1007/s10822-013-9669-z

Detection of tautomer proportions of dimedone in solution: a new approach based on theoretical and FT-IR viewpoint

Sedat Karabulut · Hilmi Namli · Jerzy Leszczynski

Received: 3 June 2013 / Accepted: 31 July 2013 / Published online: 7 August 2013

Abstract Molecular structures of stable tautomers of dimedone [5,5-dimethyl-cyclohexane-1,3-dione (**1**) and 3-hydroxy-5,5-dimethylcyclohex-2-enone (**2**)] were optimized and vibrational frequencies were calculated in five different organic solvents (dimethylsulfoxide, methanol, acetonitrile, dichloromethane and chloroform). Geometry optimizations and harmonic vibrational frequency calculations were performed at DFT 6-31+G(d,p), DFT 6-311++G(2d,2p), MP2 6-311++G (2d,2p) and MP2 aug-cc-pVDZ levels for both stable forms of dimedone. Experimental FT-IR spectra of dimedone have also been recorded in the same solvents. A new approach was developed in order to determine tautomers' ratio using both experimental and theoretical data in Lambert–Beer equation. Obtained results were compared with experimental results published in literature. It has been concluded that while DFT 6-31+G(d,p) method provides accurate enol ratio in DMSO, MeOH, and DCM, in order to obtain accurate results for the other solvents the MP2 aug-cc-pVDZ level calculations should be used for CH_3CN and $CHCl_3$ solutions.

S. Karabulut (✉) · H. Namli
Department of Chemistry, Faculty of Science and Literature, Balikesir University, Balıkesir, Turkey
e-mail: sedatk@balikesir.edu.tr; sedat@icnanotox.org

J. Leszczynski
Interdisciplinary Nanotoxicity Center, Jackson State University, Jackson, MS, USA

Keywords Dimedone · Tautomer · DFT · MP2 · FT-IR

Introduction

Tautomerization represents isomerization process vital for organic chemistry, biochemistry, and pharmacology [1–5]. The effects of solvent, temperature, intermolecular and intramolecular hydrogen bonding are driving factors of tautomerization, especially in neutral systems [6–8].

Tautomerism characterizes a dynamic equilibrium and usually occurs very fast, especially when at least one electronegative atom participates in tautomerization (e.g. nitrogen, oxygen). As a result of fast interconversion the qualitative and quantitative analysis, separation and isolation of tautomers becomes a very difficult experimental task [9–12]. In most cases it is impossible to measure the tautomer's ratios due to the high mobility of hydrogen atom in prototropic tautomerization process, even using state of art physicochemical methods [13].

Keto-enol tautomerization is one of the well-known tautomerization phenomena, especially in 1,3-dicarbonyl compounds. Structures and ratio of diketo and keto-enolic tautomers of 1,3-dicarbonyl compounds exhibit very interesting properties due to the intramolecular and intermolecular hydrogen bond effect of enolic form [14–21]. Acyclic 1,3-dicarbonyl compounds exist as a mixture of diketo and keto-enolic forms [22, 23], and the main factors that promote formation of the enol form, which is generally most abundant form, is creation of an intramolecular hydrogen bond [23]. The conjugated π system and formation of six membered ring structure are also promoting the enol form (Fig. 1). Diketo is the other stable tautomer and as it is clear from previous studies conformation of diketo

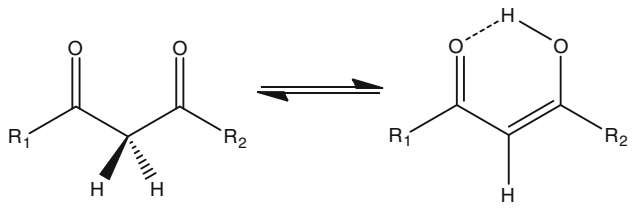

Fig. 1 Keto-enol tautomerization in acyclic 1,3-dicarbonyls

tautomer is completely different from enol structure because of strong repulsion of the localized C = O bond dipoles [24].

However, the enol tautomer of cyclic 1,3-dicarbonyl derivatives cannot form an intramolecular hydrogen bond, because of the fixed positions of carbonyls, even so the cyclic derivatives still exist as a mixture of diketo and keto-enolic forms [25–28]. Conjugated π system and hydrogen bonds between the solute molecules (or formed with the solvent) may be the reasons for the existence of keto-enolic tautomer (**2**) in cyclic 1,3-dicarbonyl (Fig. 2) systems.

Dimedone is one of the most prevalent members of cyclic 1,3-dicarbonyls and it is possible to find the applications of dimedone in many areas including industry, synthetic organic chemistry and analytical chemistry [28]. However, dimedone (**1**), cannot form intramolecular hydrogen bonds, the enol tautomer of dimedone (**2**) exists in solid state as well as in solvent media [28].

Several spectroscopic (NMR, UV, IR, HPLC, GC–MS, X-Ray) [29–33] and theoretical approaches [34] have been used for the identification of tautomeric systems. None of these methods are capable to detect the tautomers' ratio directly, except ^{1}H-NMR. Although ^{1}H-NMR technique provides the integration of hydrogen, so selected characteristics of tautomers could be revealed by such experiments, nevertheless inability of NMR time scale for the detection of fast interconversions at room temperature is a common problem. There are also other experimental techniques such the time scale of vibrational spectroscopy that is suitable for simultaneous detection of coexisting species [29, 35–37].

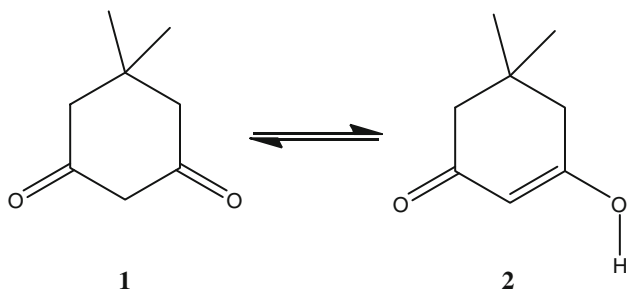

Fig. 2 Tautomerization of dimedone

Although there are several studies performed for the detection of tautomers' ratios of dimedone in solution [26, 38–41], most of these studies report different enol contents, due to the aforementioned problems in detection of tautomer proportions in solution.

A new quantitative method has been developed for detecting single component of the multicomponent mixtures quantitatively and reported previously by our group [42]. The method is based on the combination of experimental FT-IR absorbances and theoretical molar absorption coefficients (epsilon) in Lambert–Beer equation. In our previous study we have detected successfully the tautomers' proportions of acetylacetone in different solvents by using this method [42]. In the present study, this method has been applied to dimedone, which is one of the most common cyclic derivative of 1,3-dicarbonyls. We applied different levels of calculations and compared them with experimental results in order to test for the accuracy the new approach derived for detection of tautomer's ratio.

Materials and methods

All solvents and dimedone were purchased from Aldrich or Fluka as analytical purity. The vibrational absorption spectra of dimedone were recorded using a Perkin Elmer 1600 BX 2 FT-IR spectrophotometer in 0.015 mm path length CaF2 liquid cell with an average 32 scans, at 4 cm^{-1} resolution and 2 cm^{-1} interval. The concentrations of the dimedone were 0.03 mol/L for all measurements.

Calculations were performed with the Gaussian 03 [43] set of programs. The geometry optimizations and frequency calculations of tautomers of dimedone were carried out at the B3LYP/6-31+G (d,p), B3LYP/6-311++G (2d,2p) [45–49], MP2 6-311++G (2d,2p) levels of theory [49, 50] with the conductor-like polarizable continuum model (CPCM) [51] for all solvents (methanol, dimethylsulfoxide, acetonitrile, chloroform, and dichloromethane). It should be considered that the tautomer studies require a very carefully designed solution models and there are very useful methods for this [52–61]. PCM model has been used as a first step. Accuracy of this method can be increased by using different solvent modeling techniques. The default settings for Gaussian 09 for CPCM has been used (Atomic Radii: UFF, cavity type: Scaled van der Waals Surfaces (Alpha = 1.100), polarization charges: Spherical Gaussians, with point-specific exponents (IZeta = 3), dielectric constants: CH_3CN = 35.6880, $CHCl_3$ = 4.7113, DCM = 8.9300, DMSO = 46.8260, MeOH = 32.6130). MP2 aug-cc-pVDZ [62] calculations were also performed for acetonitrile and chloroform. The 2D (C–OH bond and energy) potential energy surface (step size: 10°, 36 steps) has been calculated for enol tautomer at AM1 level and the

most stable conformation detected before optimization. The harmonic vibrational frequencies have been calculated for all considered structures. Only real frequency predicted assure that the studied species are minima on the respective potential energy surfaces.

The recently developed quantitative method was reported with all details in our previous study on the acetylacetone [42]. This method is based on the application of Lambert–Beer equation for a specific frequency in infrared spectroscopy (Eq. 1).

$$A_\nu = \varepsilon_\nu l c \tag{1}$$

If the system contains more than one species the Lambert–Beer equation transforms to multi component form (Eq. 2).

$$A_{T\nu} = A_{k\nu} + A_{e\nu} = (\varepsilon_k l c_k) + (\varepsilon_e l c_e) \tag{2}$$

$A_{T\nu}$ is the total absorbance, $A_{k\nu}$ and $A_{e\nu}$ represent the absorbances of keto and enol tautomers at a specific frequency (ν). ε_k (epsilon-keto) and ε_e (epsilon-enol) are the calculated molar absorption coefficients of tautomers at maximum absorption frequency of individual absorption band, l represents the path length, ce and ck stands for the relative tautomer proportions.

The first step of the method includes calculation of the infrared spectra of each tautomer, so a suitable absorption band for individual tautomers has to be chosen as the "key band". It is essential for the key band to be as free as possible from overlapping with the absorption bands of other tautomers. Such band should also have at least a medium intensity. These kind of absorption bands can be utilized for the quantitative analysis of multi-component mixtures [42].

The second step is to record the experimental FT-IR spectra of tautomeric molecules (dimedone) in related solvent. The assignment of experimental spectra of the tautomeric mixture due to calculated vibrational frequencies of single tautomers allows choosing two absorption bands (key bands) which belong to the keto and enol tautomers and should overlap as less as possible (Fig. 3).

As it can be seen from Fig. 3a it is possible to determine key bands for keto (1604 cm^{-1}) and enol (1704 cm^{-1}) forms from the experimental spectra of the dimedone. The next step is to write the Lambert–Beer equation for both frequencies individually, considering the maximum absorbance frequencies (Eq. 3 and 4).

$$A_{1604} = 0 + A_e = 0 + (\varepsilon_e c_e l) = \varepsilon_e c_e l \tag{3}$$

$$A_{1704} = A_k + 0 = (\varepsilon_k c_k l) + 0 = \varepsilon_k c_k l \tag{4}$$

When one divides Eq. 3 by Eq. 4 the path length (l) is eliminated and one obtains a simpler equation (Eq. 5).

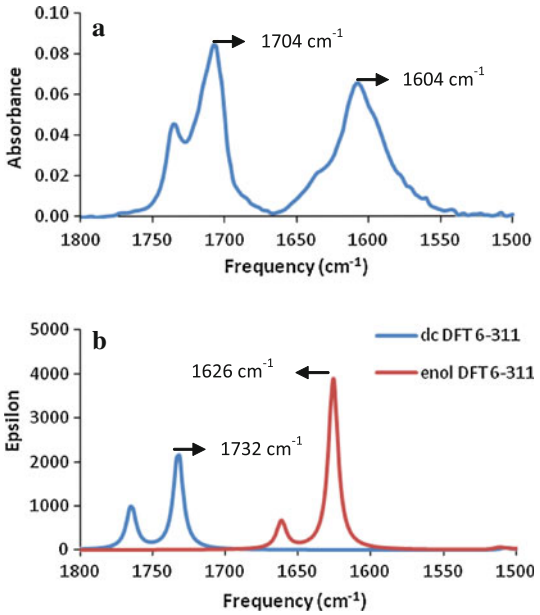

Fig. 3 **a** Experimental FT-IR spectrum of dimedone, **b** calculated and overlaid vibrational frequencies of both diketo (dc) and keto-enolic (enol) forms of dimedone between 1500 and 1800 cm^{-1} in chloroform at B3LYP 6-311 ++ G (2d, 2p) level

$$A_e/A_k = (\varepsilon_e c_e)/(\varepsilon_k c_k) \tag{5}$$

In Eq. 5 the A_{enol} and A_{keto} values will be obtained from the selected experimental key band intensities at maximum absorbance frequency. Since for most tautomeric cases the epsilon values cannot be obtained experimentally for each tautomer, because of the isolation problem of tautomers, theoretically obtained molar absorption coefficients (epsilon) were used instead.

At the first glance, using experimental and theoretical data in a single equation might not be justified because the experimental and theoretical values generally do not match. In addition, theoretical results do have different error bars than the experimental ones. However, by dividing Eq. 3 by Eq. 4 one also eleminates the difference between accuracy of theoretical and the experimental molar absorption coefficients.

The main goal of this study is to determine the tautomer ratios of dimedone in different solvents by a new technique which includes both experimental (FTIR) and theoretical data.

Results and discussions

The tautomers' ratios of dimedone have been studied by a combined experimental and theoretical method. The obtained enol concentration has been summarized in Table 1 for comparison with the literature.

Table 1 Experimental frequencies and absorbances, theoretical frequencies and epsilons, enol ratio (Ce %) (for this work and published experimental enol ratio), pure theoretical enol ratio and theoretical Gibbs free energy differences [$\Delta G^{o}_{keto} - \Delta G^{o}_{enol}$ (kcal/mol)]

		MeOH	DMSO	CH_3CN	$CHCl_3$	DCM
Experimental	Freq. keto	1710	1704	1708	1708	1708
	Abs. keto	0.0003	0.0090	0.1300	0.0800	0.2600
	Freq. enol	1602	1606	1618	1608	1614
	Abs. enol	0.3300	0.4200	0.1800	0.0600	0.0500
DFT	Theo. freq.	1619	1619	1619	1638	1629
6-31+G(d,p)	Theo. epsilon	5141.0	5205.2	5190.6	3697.4	4442.8
	Obtained Ce (%)	**99.8**	**96.0**	**40.0**	**31.5**	**10.0**
	Theo. Ce (%)	97.0	97.5	97.0	80.3	91.2
	$\Delta G^{o}_{keto} - \Delta G^{o}_{enol}$ (kcal/mol)	2.1	2.2	2.1	0.8	1.4
DFT	Theo. freq.	1608	1606	1608	1626	1617
6-311++G(2d,2p)	Theo. epsilon	5010.3	5096.9	5037.7	3888.9	4563.4
	Obtained Ce (%)	**100.0**	**96.0**	**39.9**	**29.6**	**9.7**
	Theo. Ce (%)	99.0	99.0	98.9	92.2	97.2
	$\Delta G^{o}_{keto} - \Delta G^{o}_{enol}$ (kcal/mol)	2.7	2.7	2.7	1.5	2.1
MP2	Theo. freq.	1661	1661	1661	1672	1667
6-311++G(2d,2p)	Theo. epsilon	3615.5	3651.3	3644.0	3126.9	3559.8
	Obtained Ce (%)	**99.8**	**95.6**	**37.2**	**25.3**	**8.0**
	Theo. Ce (%)	0.4	0.4	0.4	0.4	0.4
	$\Delta G^{o}_{keto} - \Delta G^{o}_{enol}$ (kcal/mol)	−3.2	−3.2	−3.2	−3.3	−3.3
MP2	Theo. freq.			1670	1675	
aug-cc-pVDZ	Theo. epsilon			2167.9	2531.2	
	Obtained Ce(%)			**49.2**	**28.6**	
	Theo. Ce (%)			0.1	0.1	
	$\Delta G^{o}_{keto} - \Delta G^{o}_{enol}$ (kcal/mol)			−4.1	−4.2	
Experimental literature Ce(%)	Theo. Ce (%)		**95–100**	**50–66**	**12–39**	**10**

Bold values are obtained relative enol concentrations for each calculation level and experimental literature results

The FT-IR spectra of dimedone have been examined between 1500 and 1800 cm^{-1} in different solvents. Calculated vibrational spectra of both tautomers (keto-enol) at different levels have been used to investigate the vibrational characteristics and molar absorption coefficients of dimedone tautomers.

Various experimentally reported enol ratios are slightly different, depending on the source of data (Table 1). Interestingly, the reported enol ratios differences are observed in chloroform and acetonitrile, while the results are consistent for dimethylsulfoxide [26, 38–41].

From the relative enol concentrations, which were obtained using the derived here approach (Table 1) it could be concluded that prediction of epsilon at different levels (DFT 6-31+G(d,p), DFT 6-311++G(2d,2p), MP2 6-311++G(2d, 2p) and MP2 aug-cc-pVDZ) does not cause a remarkable difference at obtained enol concentrations, especially in DMSO, MeOH and DCM. The obtained enol ratio does not change as a function of the method and basis set, and the obtained here results are compatible with the published experimental results (Table 1).

Thus, for the calculation of the molar absorption coefficient (ε) for the maximum frequency of selected absorption bands, it is sufficient to use DFT 6-31+G(d,p) level of theory to predict enol ratio in the considered solvents. However, as it can be gather from Table 1 our results for CH_3CN are not as accurate as for the other solvents, especially at DFT 6-31 + G(d, p), DFT 6-311++G(2d,2p) and MP2 6-311++G(2d,2p) levels. On the other hand, calculation at the MP2 aug-cc-pVDZ level provides closer results to the published enol ratio (Table 1).

The vibrational frequency of both keto and enol tautomers of dimedone were obtained at three different theory levels [DFT 6-31+G(d,p), DFT 6-311++G(2d,2p) and MP2 6-311++G(2d,2p)] in all solvents. MP2 aug-cc-pVDZ level calculations were additionally performed for CH_3CN and $CHCl_3$. The enol ratios obtained using first three levels are in good agreement, especially for DMSO,

MeOH and DCM (DMSO: 96.0, 96.0, 95.6; MeOH: 99.8, 100.0, 99.8 %; DCM: 10.0, 9.7, 8.0 %). Therefore, the MP2 aug-cc-pVDZ calculations were not performed for these solvents since the results predicted at lower levels were acceptably close to the experimental values.

The situation is slightly different for CH_3CN and $CHCl_3$ (CH_3CN: 40.0, 39.9, 37.2 %; $CHCl_3$: 31.5, 29.6, 25.3 %). Calculated results at the first three levels [DFT 6-31+G(d,p), DFT 6-311++G(2d,2p), and MP2 6-311++G(2d,2p)] are slightly different from experimental results (Table 1). As a result of this inconsistency a higher calculation level was applied (MP2 aug-cc-pVDZ) for CH_3CN and $CHCl_3$. Calculating the epsilons of tautomers with MP2 aug-cc-pVDZ provided excellent results when compared with former three levels (Table 1).

The MP2 aug-cc-pVDZ level calculation results are in harmony with literature so considering all studied systems it can be concluded that a relatively cheaper calculation [DFT 6-31+G(d, p)] can be perform for DMSO, MeOH and DCM but one should use a higher calculation level (MP2 aug-cc-pVDZ) for CH_3CN and $CHCl_3$.

The comparison of applied here improved combined method with the pure theoretical approaches has also been carried out. The Standard Gibbs free energy differences of tautomers (**1** and **2**) were calculated at room temperature (298 K) and tautomers' ratios were predicted (Table 1) (no experimental data used). An application of the DFT calculations reveals enol tautomer to be the most stable structure in all solvents. Contrary to DFT results, MP2 calculation suggested keto structure as more stable tautomer (Table 1). Application of only theoretical methods is not sufficient to calculate the relative enol concentration to be in agreement with the published experimental results. Consideration of a single, isolated tautomer in calculations, without any discrete solvent molecules may be a reason for the discrepancy between experimental and theoretical results. Neglecting in the models used in the calculation of solvent–solute and intermolecular interactions, which are important driving factors for the tautomeric equilibriums, generally yield less accurate results (Table 1).

The studied tautomeric phenomena could also be affected by various factors. While there is a conjugated π system, a mobile hydrogen and electron delocalization on enol structure (Fig. 4), polar solvents may promote dynamic structures by assisting electron shift and hydrogen transfer [63].

Application of a pure theoretical method to calculate the tautomers' ratio does not provide accurate results. On the other hand, experimental techniques have other disadvantages including time scale, necessity of isolation of a single tautomer, and cost. Thus, combination of theory and FT-IR method may be preferred, for such studies, instead of pure theoretical or experimental approaches.

As it can be seen from the Fig. 5, the overlaid spectra obtained by DFT vibrational frequency calculations (Fig. 5b) are in better agreement with the experimental FT-IR spectrum in chloroform, by means of enol frequency and intensity, than MP2 level spectra. In these relatively non-polar solvents the enol tautomer may benefit more from interaction with another enol tautomer rather than interaction with nonpolar solvent molecules. This interaction may cause shifts of C = C and C = O absorption bands and their overlap on FT-IR [28]. There is only a small shoulder at 1736 cm^{-1} recorded experimentally, which may belong to monomeric enol content.

In CH_3CN there is a clear difference of frequency and intensity between experimental spectra and calculated vibrational frequency with first three levels [DFT 6-31+G(d,p), DFT 6-311++G(2d,2p), and MP2 6-311++G(2d,2p)] at carbonyl region (Fig. 6). Enol tautomer may benefit more from interaction with polar solvent (CH_3CN) molecules rather than from interaction with other enols. Thus the monomeric vibrational characteristic of enol becomes predominant so C = C and C = O stretching

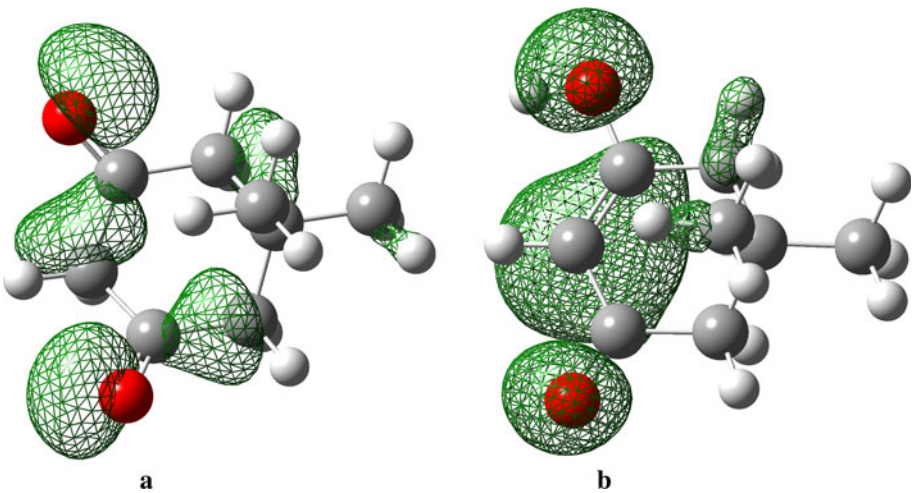

Fig. 4 Negative isosurfaces of diketo (**a**) and keto-enol (**b**) structures (Isovalue: 0.02)

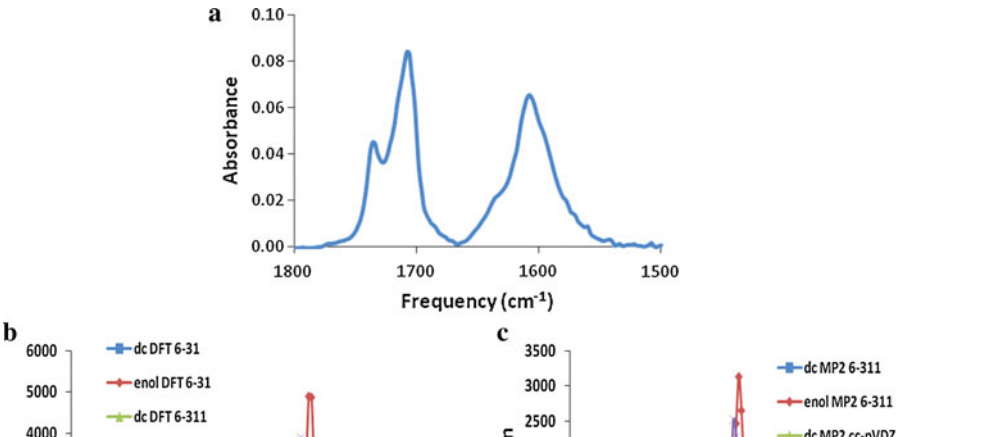

Fig. 5 Experimental FT-IR spectrum of dimedone (**a**) calculated and overlaid vibrational frequencies of diketo (dc) and keto-enolic (enol) tautomers at DFT (**b**) and MP2 (**c**) levels between 1500 and 1800 cm^{-1} in chloroform

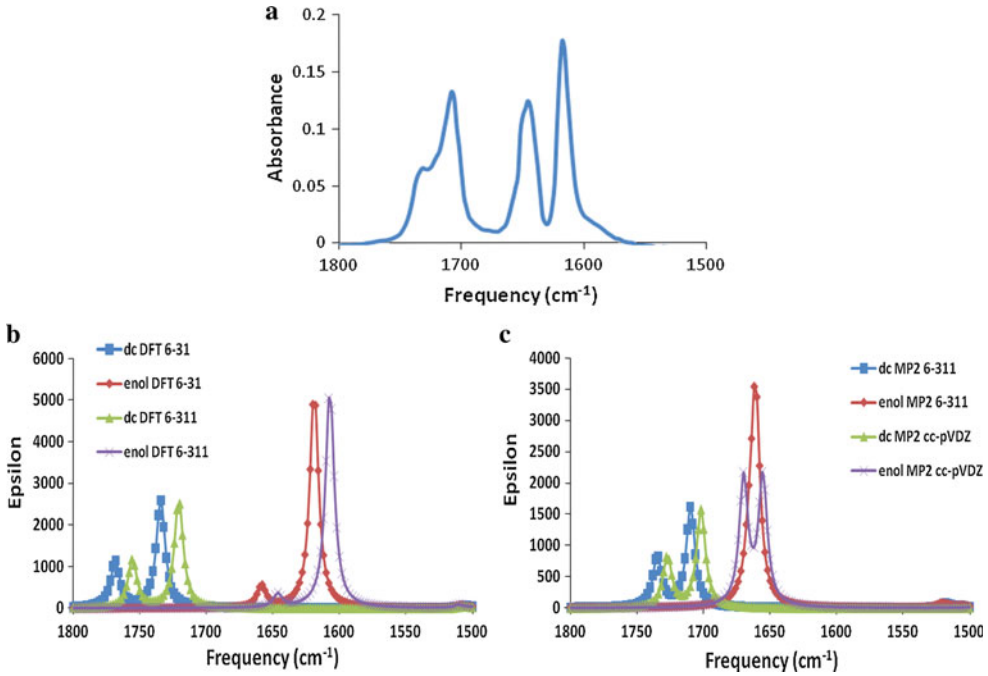

Fig. 6 Experimental FT-IR spectrum of dimedone (**a**) and calculated vibrational frequencies of both diketo (dc) and keto-enolic (enol) tautomers between 1500 and 1800 cm^{-1} in DFT (**b**) and MP2 (**c**) levels in acetonitrile

bands separate. As it can be seen from Fig. 6c the C = C and C = O stretching bands of vibrational spectrum of enol tautomer calculated at MP2 aug-cc-pVDZ level are very similar to experimental spectrum. Lower level calculations failed to properly predict peak intensities at calculated vibrational spectrum of enol structure in CH_3CN. This conclusion is supported by the similarity between the experimental (Fig. 6a) and theoretical spectra (Fig. 6c) and the agreement between the experimental and obtained enol ratio (Table 1) with the new developed method.

Conclusion

The presented here method is feasible to solve the detection problem of relative concentrations of multicomponent

systems (dimerization, tautomerization, rotamerization, etc.) in solvent media without necessity of isolation of components. The widely used methods suffer from various disadvantages including fast transformation and inability of time scale of NMR. The combination of theoretical calculations and experimental vibrational spectroscopy is easier, cheaper and faster than NMR technique and there are no solvent restrictions in the proposed approach.

It has been concluded that the calculation of epsilon with smaller basis sets (DFT 6-31+G(d,p)) yields acceptable results in DMSO, MeOH and DCM but relatively more expensive level (MP2 aug-cc-pVDZ) is needed to calculate accurate enol concentration in CH_3CN and $CHCl_3$.

References

1. Watson JD, Crick FHC (1953) Nature 171:737–738
2. Löwdin PO (1965) Adv Quantum Chem 2:213–360
3. Pullman B, Pullman A (1971) Adv Heterocycl Chem 13:77–159
4. Topal MD, Fresco JR (1976) Nature 263:285–289
5. Raczynska ED, Kosinska W, Osmialowski B, Gawinecki R (2005) Chem Rev 105:3561–3612
6. Minkin VI, Olekhnovich LP, Zhdanov YA (1981) Acc Chem Res 14(7):210–217
7. Cruz-Cabeza AJ, Schreyer A, Pitt WR (2010) J Comput Aided Mol Des 24:575–586
8. Claisen L (1896) Liebigs Ann Chem 291:25–137
9. Seckarova P, Marek R, Malioakova K, Kolehmainen E, Hockova D, Hocek M, Sklenar V (2004) Tetrahedron Lett 45:6259–6263
10. Katritzky AR, Hall CD, El-Gendy BEM, Draghici B (2010) J Comput Aided Mol Des 24:475–484
11. Cook AG (1998) Enamines, 2nd ed. Marcel Dekker, New York
12. Reichardt C (1979) Solvent effects in organic chemistry. Verlag Chemie, Weinheim, Germany, New York
13. Galstyan G, Knapp EW (2012) J Phys Chem A 116:6885–6893
14. Takasuka M, Saito T, Nakai H (1996) Vib Spectrosc 13:65–74
15. Lu J, Han B, Yan H (1999) J Supercrit Fluids 15:135–143
16. Jios JL, Duddeck H (2000) Magn Reson Chem 38:512–514
17. Iglesias E (2004) Curr Org Chem 8:1–24
18. Egan W, Gunnarsson G, Bull TE, Forsen S (1977) J Am Chem Soc 99:4568–4572
19. Hibbert F, Emsnley J (1990) Adv Phys Org Chem 26:255–379
20. Kereselidze JA, Zarqua TS, Kikalishvili TJ, Churgulia EJ, Makaridze MC (2002) Russ Chem Rev 71:993–1003
21. Cornago P, Claramunt RM, Bouissane L, Alkorta I, Elguero J (2008) Tetrahed 64:8089–8094
22. Knorr L (1896) Liebigs Ann Chem 293:70–120
23. Lacerda V Jr, Constantino MG, da Silva GVJ, Neto AC, Tormena CF (2007) J Mol Struct 828:54–58
24. Pocker Y, Spyridis GT (2002) J Am Chem Soc 124:10373–10380
25. Emsley J (1984) Struct Bond 57:147-191
26. Yogev A, Mazur Y (1967) J Org Chem 32:2162–2166
27. Richa AM, Diaz GM, Nathan PJ (1996) Appl Spectrosc 50: 1408–1412
28. Sigalov M, Shainyan B, Krief P, Ushakov I, Chipanina N, Oznobikhina L (2011) J Mol Struct 1006:234–246
29. Emsley J, Neville JF (1987) J Mol Struct 161:193–204
30. Coussan S, Ferro Y, Trivella A, Rajzmann M, Roubin P, Wieczorek R, Manca C, Piecuch P, Kowalski K, Wloch M, Kucharski SA, Musial M (2006) J Phys Chem A 110:3920–3926
31. Claramunt RM, Lopez C, Santa Maria MD, Sanz D, Elguero J (2006) Prog Nucl Magn Reson Spectrosc 49:169–206
32. Boese R, Antipin MY, Blalser D, Lyssenko KA (1998) J Phys Chem B 102:8654–8660
33. Moriyasu M, Kato A, Hashimoto Y (1986) J Chem Soc Perkin II II:515–520
34. Chen XB, Fang WH, Phillips DL (2006) J Phys Chem A 110:4434–4441
35. Karabulut S, Namli H, Mella M (2011) Vib Spec 57:294–299
36. Raczynska ED, Kosinska W (2005) Chem Rev 105:3561–3612
37. Yaylayan VA, Ismail AA, Mandeville S (1993) Carbohydr Res 248:355–360
38. Moriyasu M, Kato A, Hashimoto Y (1988) Bull Chem Soc Jpn 61:2955–2956
39. Mills SG, Beak P (1985) J Org Chem 50:1216–1224
40. Majumdar P, Mohanta P, Behera RK, Behera AK (2013) Synt Comm1 43:899–914
41. Cremlyn RJ, Osborne AG, Warmsley JF (1996) Spectrochim Acta A 52:1433–1454
42. Karabulut S, Namlı H (2012) J Mol Struct 1024:151–155
43. Gaussian 03, Revision C.02, Frisch MJ, Trucks GW, Schlegel HB, Scuseria GE, Robb MA, Cheeseman JR, Montgomery Jr JA, Vreven T, Kudin KN, Burant JC, Millam JM, Iyengar SS, Tomasi J, Barone V, Mennucci B, Cossi M, Scalmani G, Rega N, J Mol ModelPetersson GA, Nakatsuji H, Hada M, Ehara M, Toyota K, Fukuda R, Hasegawa J, Ishida M, Nakajima T, Honda Y, Kitao O, Nakai H, Klene M, Li X, Knox JE, Hratchian HP, Cross JB, Bakken V, Adamo C, Jaramillo J, Gomperts R, Stratmann RE, Yazyev O, Austin AJ, Cammi R, Pomelli C, Ochterski JW, Ayala PY, Morokuma K, Voth GA, Salvador P, Dannenberg JJ, Zakrzewski VG, Dapprich S, Daniels AD, Strain MC, Farkas O, Malick DK, Rabuck AD, Raghavachari K, Foresman JB, Ortiz JV, Cui Q, Baboul AG, Clifford S, Cioslowski J, Stefanov BB, Liu G, Liashenko A, Piskorz P, Komaromi I, Martin RL, Fox DJ, Keith T, Al-Laham MA, Peng CY, Nanayakkara A, Challacombe M, Gill PMW, Johnson B, Chen W, Wong MW, Gonzalez C, Pople JA (2004) Gaussian Inc, Wallingford, CT, USA
44. Hehre WJ, Radom L, Schleyer PvR, Pople JA (1986) Ab initio molecular theory. Wiley, New York
45. Jensen F (1999) Introduction to computational chemistry. John Wiley & Sons, London
46. Parr RG, Yang W (1989) Density functional theory of atoms and molecules. Oxford University Press, New York
47. Lee C, Yang W, Parr RG (1988) Phys Rev 37:785–789
48. Becke AD (1988) Phys Rev B 38:3098–3100
49. Moller C, Plesset MS (1934) Phys Rev 46:618–622
50. Cremer D (1998) In: Schleyer PvR (ed) Encyclopedia of computational chemistry. John Wiley and Sons, New York
51. Barone V, Cossi M (1998) J Phys Chem A 102:1995–2001
52. Ellingson BA, Skillman AG, Nicholls A (2010) J Comput Aided Mol Des 24:335–342
53. Soteras I, Orozco M, Luque FJ (2010) J Comput Aided Mol Des 24:281–291
54. Klimovic PV, Mobley DL (2010) J Comput Aided Mol Des 24:307–316
55. Riberio RF, Marenich AV, Cramer CJ, Truhlar DG (2010) J Comput Aided Mol Des 24:317–333
56. Kast SM, Heil J, Güssregen S, Schmidt KF (2010) J Comput Aided Mol Des 24:343–353
57. Klamt A, Diedenhofen M (2010) J Comput Aided Mol Des 24:357–360
58. Meunier A, Truchon JF (2010) J Comput Aided Mol Des 24:361–372
59. Purisima EO, Corbeil CR, Sulea T (2010) J Comput Aided Mol Des 24:373–383

60. Nicholls A, Wlodek S, Grant JA (2010) J Comput Aided Mol Des 24:293–306
61. Geballe MT, Skillman AG, Nicholls A, Guthrie JP, Taylor PJ (2010) J Comput Aided Mol Des 24:259–279
62. Dunning TH Jr (1989) J Chem Phys 90:1007–1023
63. Lu J, Han B, Yan H (1999) J Supercr Fl 15:135–143